Combustive, Postcombustive, and Tropospheric Butadiyne Oxidation by O2, Following Initial HO Attack. Theoretical Study

Combustive, Postcombustive, and Tropospheric Butadiyne Oxidation by O_2, Following Initial HO Attack. Theoretical Study.

Andrea Maranzana, Giovanni Ghigo, and Glauco Tonachini*

Dipartimento di Chimica, Università di Torino, via Pietro Giuria, 7, I-10125 Torino, Italy

Abstract.

Butadiyne (diacetylene, HC_4H) is produced during combustions, and has been quantified in different flames as well as a biomass burning emission. Its reaction with the hydroxyl radical, $HO(^2\Pi_{3/2})$, under combustion conditions, was investigated in a thorough RRKM study by J. P. Senosiain, S. J. Klippenstein, and J. A. Miller (*Proc. Comb. Inst.* **2007**, *31*, 185–192). The present Density Functional Theory (DFT) study focuses on the mechanism of further oxidation by $O_2(^3\Sigma_g^-)$. The DFT(M06-2X)/cc-pV*TZ* reaction energy hypersurface for the system $C_4H_2/HO^\bullet/O_2$ is studied to define a variety of reaction pathways, and the relevant thermochemistry for temperatures ranging from 200 to 2500 K is assessed, thus encompassing combustive, post-combustive, and tropospheric conditions. Energies are then recomputed at the coupled cluster level [CCSD(T)/ cc-pV*TZ*], and combined with the DFT thermochemistry. Finally, the role of the different reaction channels is assessed by RRKM-ME simulations in the same temperature range for P = 1 atm, to comprise the situation of emission in the troposphere and those pertaining to different flames. This shows that, when considering HO addition to the triple bond, dioxygen takes part in C_4H_2 oxidation with higher efficiency at lower temperatures, whereas, as T rises, the O_2 adducts are inclined to redissociate: for instance, a 50% redissociation is estimated at T=1800 K. For 200 < T < 1100 K, two polycarbonyl products (CHO.CO.C≡CH and CHO.CO.CH=C=O) and two fragmentation products (HCOOH plus $OC^\bullet$–C≡CH) are the main species predicted as products from the addition channel (fragmentation is entropy-favored by higher T values). However, at higher temperatures, an initial H abstraction by HO can give the butadiynyl radical ($HC_4^\bullet$) as the starting point for subsequent dioxygen intervention. Then, new pathways opened by O_2 addition become accessible and bring about fragmentations mainly to $HC_3^\bullet + CO_2$ and also to $HC_3^\bullet O + CO$.

Keywords: 1) butadiyne; 2) combustion; 3) tropospheric oxidation; 4) hydroxyl; 5) dioxygen; 6) DFT; 7) RRKM

* corresponding author. Address: Dipartimento di Chimica, Università di Torino, Corso Massimo D'Azeglio 48, I-10125 Torino, Italy.

E-mail addresses. Andrea Maranzana: andrea.maranzana@unito.it - Giovanni Ghigo: giovanni.ghigo@unito.it
Glauco Tonachini: glauco.tonachini@unito.it / phone: ++39-011-6707648 / fax: ++39-011-2367648

Proposed running title: butadiyne oxidation

Introduction.

Polyynes have been detected under very different physical and chemical conditions, ranging from combustion situations[1] to interstellar, protostar cloud, or planetary environment,[2] They had already been considered, at an earlier time, as important combustion intermediates by Homann and Wagner,[3] and then by Krestinin,[4] who proposed the ring closure-radical breeding polyyne-based mechanism for PAH and soot growth. Their possible role in the synthesis of an aromatic ring (o-benzyne) has been reviewed recently.[5] The oxidation of polyynes at combustion temperatures could also bear some relevance to the formation of oxidized PAHs and soot platelets, if it is assumed that oxidation can take place all through their synthesis. Polyyne oxidation in a combustion situation might be likely initiated by small reactive radicals, as hydrogen and oxygen atoms, or hydroxyl, that can be present in significant amounts.[6] Conversely, once polyynes are emitted in the tropospheric environment their fate is determined by a lower-T oxidation processes modulated also by the very different concentrations of the reactive species which can start off the oxidation process.

Among polyynes, butadiyne (HC≡C–C≡CH, also called diacetylene) is an important intermediate[7] in combustion processes[8,9,10] (related to this, we can also mention two studies on its pyrolysis[11] and oxidation[12]). It is present in the highest concentration among polyyne molecules[13] (hence eventually emitted in the troposphere). Its maximum mole fraction χ_{max} in the oxidation zone of premixed ethyne,[14] benzene,[15] toluene,[16] cyclopentene,[1,17] allene,[1] propyne,[1] or gasoline[18] flames has been measured in the range χ_{max} = 2–6 x 10^{-3}, or up to in a methane flame.[19] Butadiyne has also been quantified as an emission released in the troposphere as a consequence of vegetative fuel combustion.[20] We can also mention that butadiyne has been identified in astrochemical investigations.[21] However, though O_2 has been recently detected in Orion by a *Herschel* measurement,[22] and the presence of oxygen under different forms on Titan discussed,[23] the importance of oxidation processes in those environments appears dubious.

The C_4H_2 + $HO^{\cdot}$ reaction, in particular, has been studied experimentally in a limited number of investigations,[24,25,26] and theoretically by Senosiain, Klippenstein, and Miller (hereafter referred to as SKM) in a thorough RRKM study under conditions relevant to combustion.[27a] The purpose of the present investigation is to extend the study (1) beyond the reaction with hydroxyl, focusing on the subsequent dioxygen intervention, and (2) to situations ranging from combustion to post-combustion (emission in the environment), and then tropospheric oxidation, to assess under which conditions dioxygen addition can best proceed to oxidation products. In the end, the likelihood of the reaction pathways so defined will be assessed theoretically over a range of temperatures (see Method section).

The initial intermediates which form upon a hydroxyl radical attack onto butadiyne are shown in Scheme 1, and are part of the study by SKM. Either the addition to the carbon-carbon triple bond takes place (to C1 or C2), or H abstraction (shown by SKM to gain some importance for temperatures beyond 1200 K). The radical originating from hydroxyl addition to C2 is less stable than **A1**, is obtained significantly less easily, hence has not be considered any further.[27a,28]

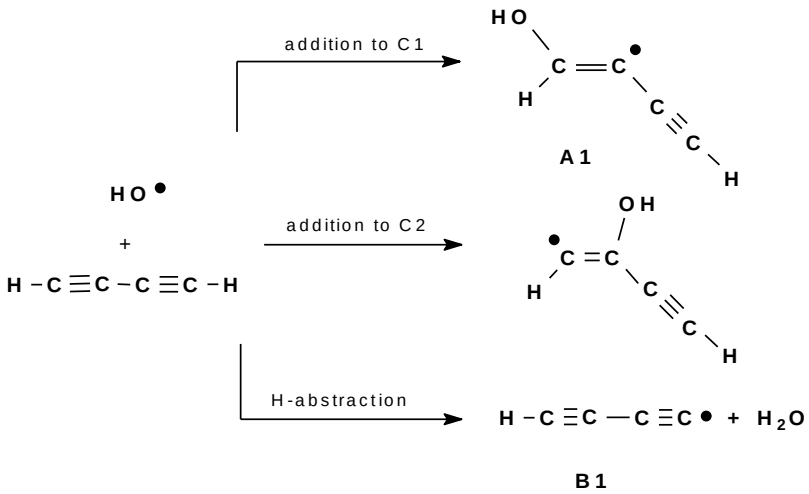

Scheme 1. Initial steps of ther hydroxyl radical attack onto butadiyne.

Theoretical Method.

All stationary points on the energy hypersurface, *i.e.* minima and first order saddle points, corresponding to transition structures (TS), were determined by gradient procedures[29] within the Density Functional Theory (DFT),[30] and making use of the M06-2X[31] functional. Dunning's correlation-consistent polarized valence triple-ζ basis set cc-pV*TZ*[32] was used thoughout in the DFT optimizations. The nature of the critical points (and the thermochemistry) was assessed by vibrational analysis. The M06-2X/cc-pV*TZ* thermochemical corrections gave estimates of the zero point vibrational energy (ZPE), by which the relative energies were corrected to obtain ΔE_{ZPE} (= ΔE + ΔZPE) values, enthalpy (ΔH) and Gibbs free energy (ΔG) differences (energetics in kcal mol^{-1}). The thermochemistry was assessed in all cases at temperatures ranging from troposheric values up to those typical of combustion (T = 200-2500 K). The DFT energetics is reported in the Supporting Information, section 3. The relevant critical points were selected, for comparative purposes, for a series of coupled cluster calculations, carried out at the CCSD(T) level[33] with the cc-pv*TZ* basis set. These energy values were combined with the DFT(M06-2X)/cc-pV*TZ* thermochemistry, to define the ΔE_{ZPE} values reported in the Schemes, and to ascertain the more viable evolution paths of the reacting system. Geometry optimization and thermochemistry calculations were carried out by using the GAUSSIAN 09 system of programs.[34]

The Rice Ramsperger Kassel Marcus (RRKM) theory[35,36] was then used to obtain the distribution of reaction products. In order to obtain these distributions as functions of time, RRKM and Master Equation (ME) calculations were carried out by using Multiwell program suite.[37,38,39] It allows to calculate sum and densities of states, then obtains microcanonical rate constants according to RRKM theory, and finally solves the master equation. Corrections for quantum tunneling were included for all hydrogen transfer reactions (not H dissociations) by incorporating the corrections for one-dimensional unsymmetrical Eckart barriers.[40] Internal rotations were treated approximately as a symmetric hindered internal rotation.[41] MultiWell stores densities and sums of states in double arrays: the lower part of the array consisted of 800 array elements which ranged in energy from 0 cm^{-1} to 3995 cm^{-1}. The higher energy part of the double array consisted of 200 elements ranging in energy from 0 cm^{-1} to 150000 cm^{-1} with an energy spacing of 753 cm^{-1}. The Lennard-Jones parameters necessary for the collision frequency calculations, assumed to be the same for all the structures, were: σ= 5.1 Å, and ε/k_B = 535 K. For the N_2 collider: σ(A) = 3.75 Å, and ε/k_B = 80 K. Energy transfer, dependent from the temperature, was treated by assuming the exponential-down model for collision step-size distributions: E_{down}= 250 cm^{-1} • $(T/298)^{-0.85}$, as suggested by SKM.[27a] Rate constants were calculated in the range 200-2500 K. In the present work, the number of stochastic trials was set to 10^7, for 300 collisions. Simulations were carried out at P= 1 atm of N_2 buffer gas, relevant to combustions and low low troposphere.

Results and Discussion.

As said above, the present study mainly investigates the effects of dioxygen addition to the initial intermediates which form upon a first hydroxyl radical attack onto butadiyne (Scheme 1). The outcome of the hydroxyl radical attack onto butadiyne was the subject of the mentioned SKM study,[27a] and will not be recalled here. In the reaction steps studied here, beginning with dioxygen intervention, the pathways that originate from the HO adduct **A1** will connect structures labeled as **An** (Scheme 2 and subsection 1.1), whilst those originated by the butadiynyl radical **B1** will connect structures labeled as **Bn** (Scheme 3 and subsection 1.2). Only the radical **A1**, originating from hydroxyl addition to C1, will be considered.[28] For some radical intermediates presenting a delocalized unpaired electron, spin densities are reported in the Supporting Information, section 1.

1. Reaction pathways opened by HO addition.

1.1 Dioxygen addition. We proceed by considering O_2 addition to the initial hydroxyl-butadiyne adduct **A1** (Scheme 2), whose presence has been shown t o be substantial within the temperature range taken into consideration by SKM (Figure 7 in ref. 27a). The relevant coupled cluster energetics is reported in Scheme 2.

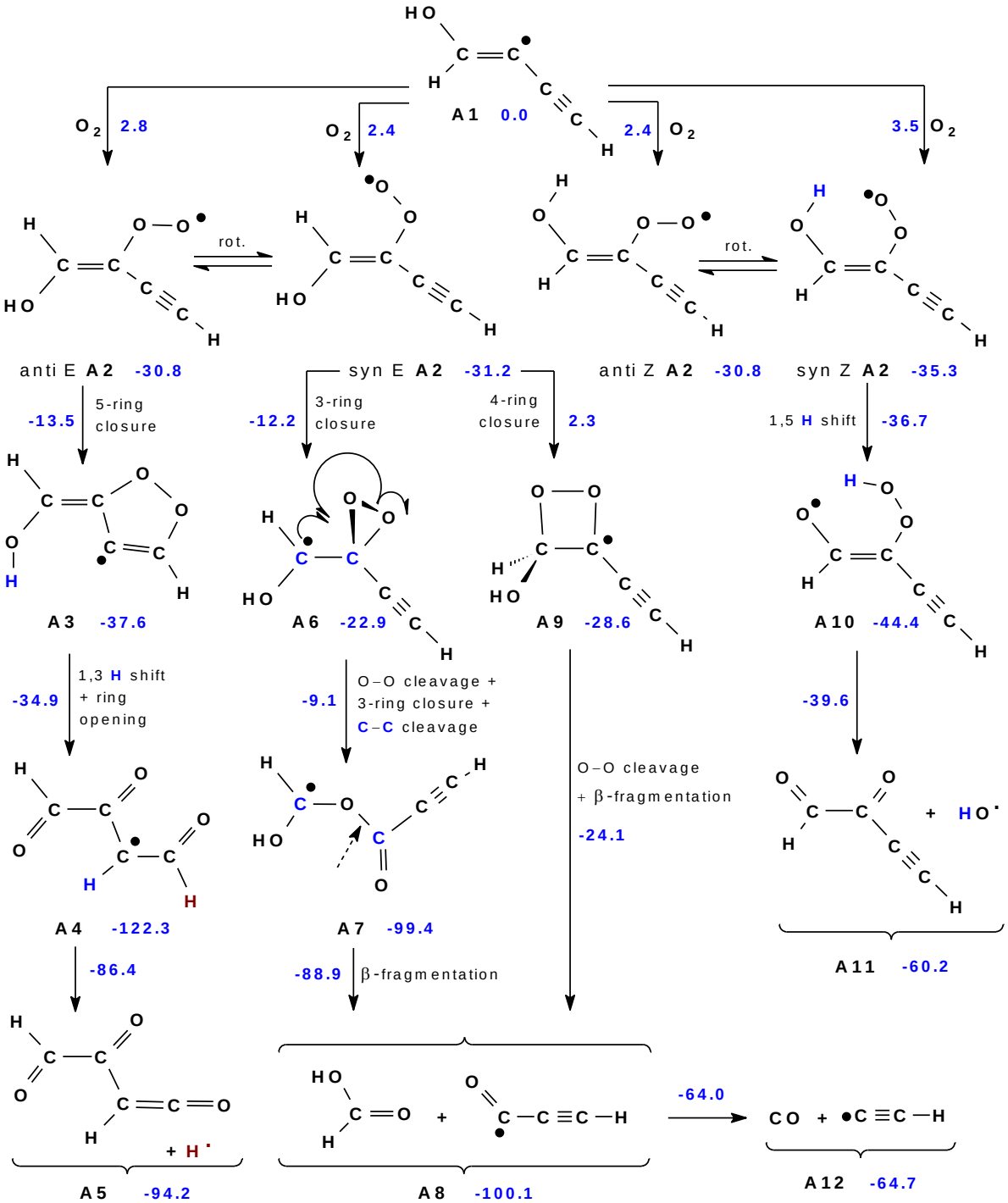

Scheme 2. Pathways stemming from dioxygen addition to the stabler initial HO-butadiyne adduct. Labels *syn* and *anti* refer to the C=C–O–O dihedral angle, E and Z to the positions of the HO and OO substituents with respect to the double bond. ΔE_{ZPE} values (see Method section) are reported as blue figures, referred to the initial hydroxyl adduct.

Dioxygen addition to the adduct **A1** forms two initial hydroxyl-peroxyl radical adducts **A2**, for which the Z and E symbols refer to the relative positions of the hydroxyl and peroxyl substituents. Thus we get: *syn* and *anti* Z-**A2** (two rotamers), or *syn* and *anti* E-**A2** (two other rotamers), where *syn* and *anti* correspond to O–O–C=C dihedral angles of 0° and 180°, respectively. From anti E-**A2** a 5-ring closure leads to the radical **A3**, and a subsequent H shift to **A4**. From **A4**, a H loss gives the tri-carbonyl closed shell product **A5**. From syn E-**A2** two pathway depart, that converge in the end to the same outcome. If a 3-ring closure takes place, it gives the peroxirane **A6**. When the peroxy bond in **A6** cleaves, another 3-ring closure occurs, to form an epoxy ring, as indicated by the curly arrows, but the cleavage of the epoxy ring C–C bond takes place concertedly (blue carbons). By these three events, the radical **A7** forms. Through a final fragmentation, formic acid and an acyl radical are produced, collectively labeled as **A8**. As an alternative to the step '*syn* E **A2**-**A6**', a 4-ring closure gives the dioxetane-like radical **A9**. Peroxy bond cleavage is accompanied concertedly by cleavage of the opposite C–C bond, giving again the fragments **A8**. Still another pathway departs from *syn* Z **A2** (*anti* Z **A2** transforms rapidly to its stabler *syn* rotamer), beginning with a H shift to give the hydroperoxide radical **A10**, which loses a hydroxyl radical and leaves the closed shell product **A11**. **A5**, **A8**, and **A11** have a particular importance, as will be seen presently in section 3.1.

1.2 Reaction pathways opened by H abstraction. An alkyne hydrogen is in itself hard to abstract, as suggested by its homolytic dissociation enthalpy, D_e ~ 125 kcal mol^{-1}. However, as commented by SKM, hydroxyl can perform abstraction from butadiyne competitively above 1200 K.[27a] Pathways which originate from the ensuing butadiynyl radical **B1** are shown in Scheme 3.

Direct fragmentations of the radical **B1**, to give the ethynyl radical plus C_2 or C_4, are unlikely because these diradicals are high in energy. Dioxygen addition to the localized radical site of **B1** produces **B2**, which in turn undergoes ring closure and gives the peroxirane-like radical **B3**. Peroxy bond homolytic cleavage in **B3** (a, Scheme 3) gives concertedly closure of an epoxide ring (b) and produces **B4**, with a significant stability gain.[42] Actually, upon the dioxirane-like ring opening, two equivalent ring closures can take place (b, b', Scheme 4): either oxygen can give ring closure, while the other remains as an oxyl/carbonyl substituent of the epoxide ring (see the resonance structures for **B4**). While **B3** is C_{2v}, the ring opening TS slightly departs from it, being actually C_1. The symmetry lowering is necessary, in order to have a transition structure instead of a cusp, because **B3** and **B4** have different wavefunction symmetry. The former is symmetric with respect to the molecular plane, since the unpaired electron lies on it. The latter, by contrast, has an enol radical-like π system extended on the [C=C–O$^\bullet$ ↔ $^\bullet$C–C=O] atoms. Therefore, its wavefunction is antisym-

metric. The real crossing in C_{2v} symmetry then becomes an avoided crossing if the symmetry is lowered, and consequently this is a case of conical intersection.

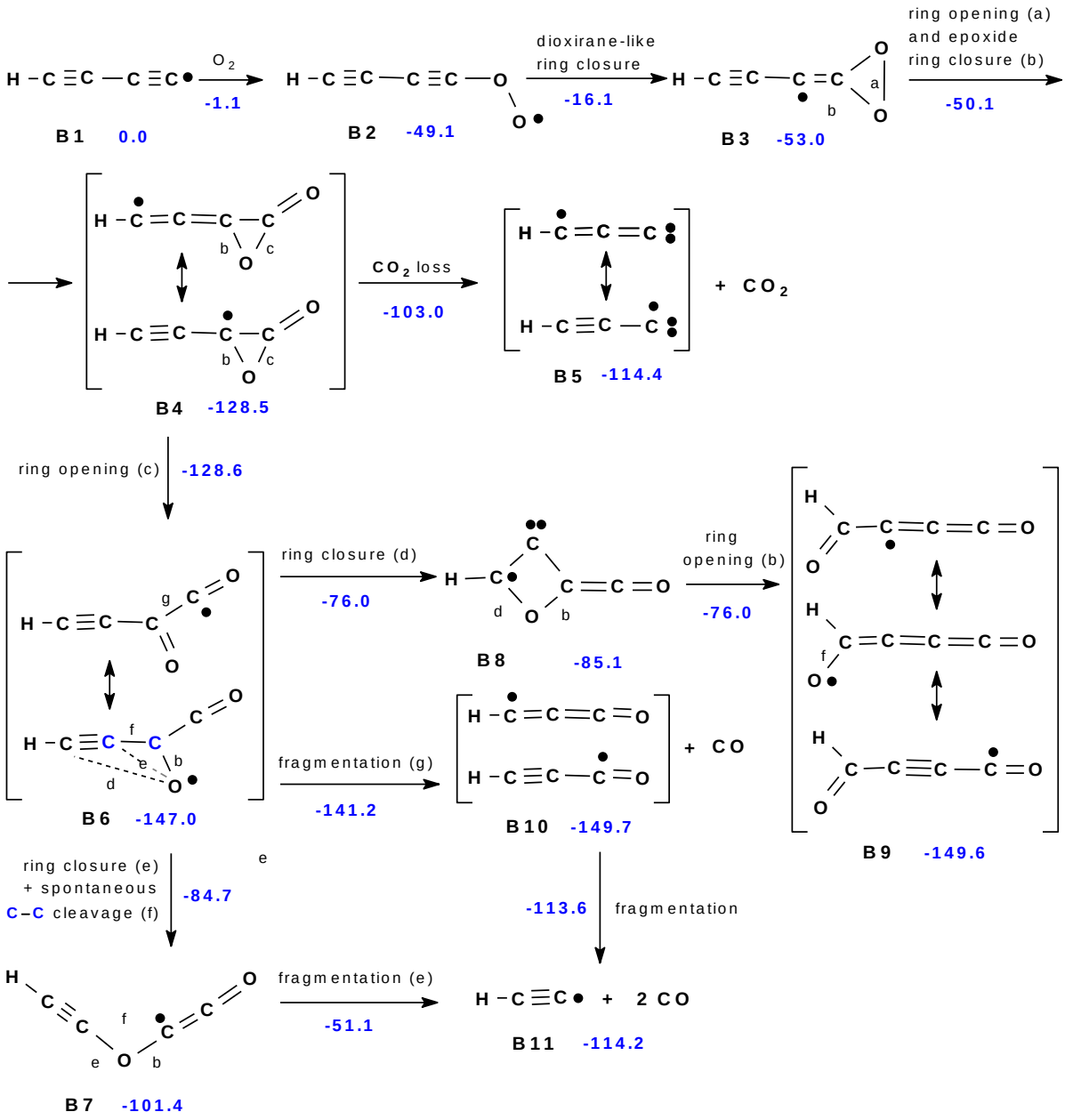

Scheme 3. Higher-temperature pathways from dioxygen addition to the butadiynyl radical, which is in turn generated by initial H-abstraction operated by HO on HC_4H. ΔE_{ZPE} values (see Method section) are reported as blue figures, referred to the butadiynyl radical plus dioxygen separate reactants.

A bifurcation of the reaction pathways must accordingly be present, with two rather early transition structures, each one made up by to enantiomers,[43] which can however be mentally seen as distinct regarding the involvement of the individual oxygen atoms (an isotopic substitution for one O would make them distinguishable). They are represented in Scheme 4, for clarity, associated to the unique cleavage a and one of two alternative closures b and b'.

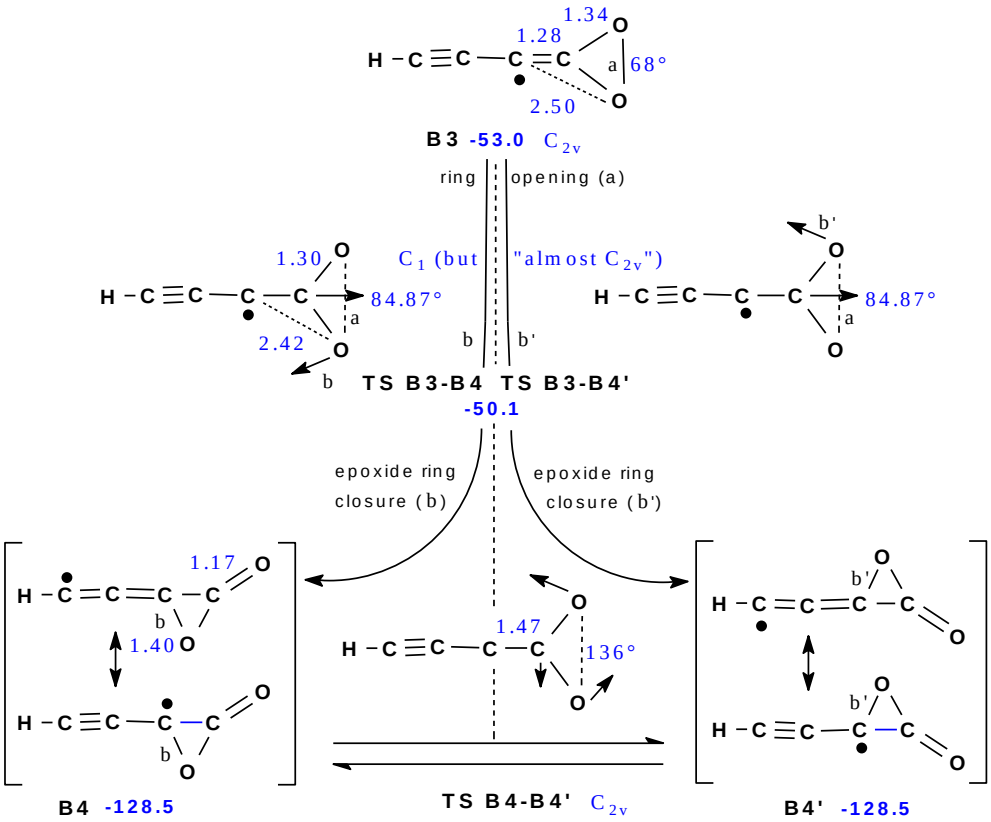

Scheme 4. Connection of **B3** with **B4** through a bifurcation. The vertical dashed line hints to the presence of a ridge, which separates the two equivalent downhill pathways towards **B4** and **B4'**. Along the bifurcation and the ridge, down to the interconversion TS **B4**-**B4'**, the C_{2v} symmetry is maintained (only approximately in TS **B3**-**B4**, which is actually C_1). See note 43.

The bifurcation to TS **B3**-**B4** and TS **B3**-**B4'** thus entails, past the transition structures, two equivalent all-downhill pathways that lead to the two equivalent epoxy-oxyl/carbonyl intermediates, **B4** and **B4'**. The two superimposable or enantiomeric[43] intermediates can in principle interconvert through TS **B4**-**B4'** (again C_{2v}).

From **B4** (Scheme 4), CO_2 loss is possible. As far as ΔE_{ZPE} values are considered, it occurs less easily than formation of **B6**. We can nevertheless expect that a growing T could greatly favor it. As an alternative, the epoxide ring in **B4** can open again, from the side closer to the CO group (cleavage of the bond labeled "c"), resulting in an overall oxygen atom migration from the formerly terminal carbon atom to its neighbor.

The open-chain resonant radical **B6** so obtained is rather stable. It can give a fragmentation, as **B6**-**B10**(-**B11**), or further rearrange (as **B6**-**B7** or **B6**-**B8**-**B9**). If it undergoes a fragmentation, a delocalized radical plus carbon monoxide form (collectively indicated as **B10**). This radical might as well further fragment to the ethynyl radical plus CO again (**B11**). If instead **B6** undergoes a rearrangement, this can take place in two different ways. The migrating oxygen atom can in one case proceed to the next carbon, forming the bond labeled "d" in **B7**, in which step also one C–C bond cleaves concertedly, and therefore an ether functionality forms. This intermediate, rather

high in energy compared to the previous one, can undergo a fragmentation to ethynyl radical and the putative OCCO closed shell molecule, which is however unstable with respect to two carbon monoxide moieties, and dissociates spontaneously (again to the dissociation limit **B11**). A different migration of the same oxygen can take place by skipping the high minimum of **B7**, via ring closure (formation of bond "f") to produce an oxetene-like system, **B8**. If now bond "b" cleaves, another open-chain intermediate forms, **B9**, quite stable again. The steps from **B6** to **B7** and **B8** do not seem too promising.

3. RRKM analysis.

Two distinct RRKM-ME simulations are carried out (at P = 1 atm). One starts from the HO addition intermediate **2**, which has been shown by SKM to be present in significant amounts at all temperatures considered (Figure 7 in ref. 27a), though dropping almost linearly from ca. 80% at 1400 K to ca. 10% at 2400 K. The other one starts instead from the butadiynyl radical **B1**. We begin with the former.

3.1 Reaction pathways started by hydroxyl addition to butadiyne. The RRKM-ME results show that the two initial hydroxyl-peroxyl radical adducts **A2** (on the whole *syn* and *anti* rotamers of Z-**A2** plus *syn* and *anti* rotamers[44] of E-**A2**) give back-reaction to the reactants **A1** and O_2 to an extent which at higher temperatures becomes significant. At lower temperatures the back-reaction is not favored. Since this effect is not observable in the yield experiments, the computational results pertaining to product yields reported here have been corrected for it. The product *net reaction yields* reported in Figure 1 as continuous lines exclude the re-dissociation to **2** and O_2: these individual yields add up to 1. The dashed line represents the sum of the products that survive to redissociation to **A1** + O_2 (1 – back reaction), or, said differently, of **A2** + all other products derived from it. We stress that its value too is expressed as ranging in principle from 0 to 1, as is true for each of the continuous lines, but here it stays alone (in other words, its values have not to be added to those of the products). It has been reported to convey an information about the importance of the product formation yields, which is somewhat declining as T rises. Two entrance channels are present (Z-**A2** and E-**A2**).[44] Separate simulations were carried out, then the total yields were calculated by weight-averaging the individual channels (see the Supporting Information, section 2).

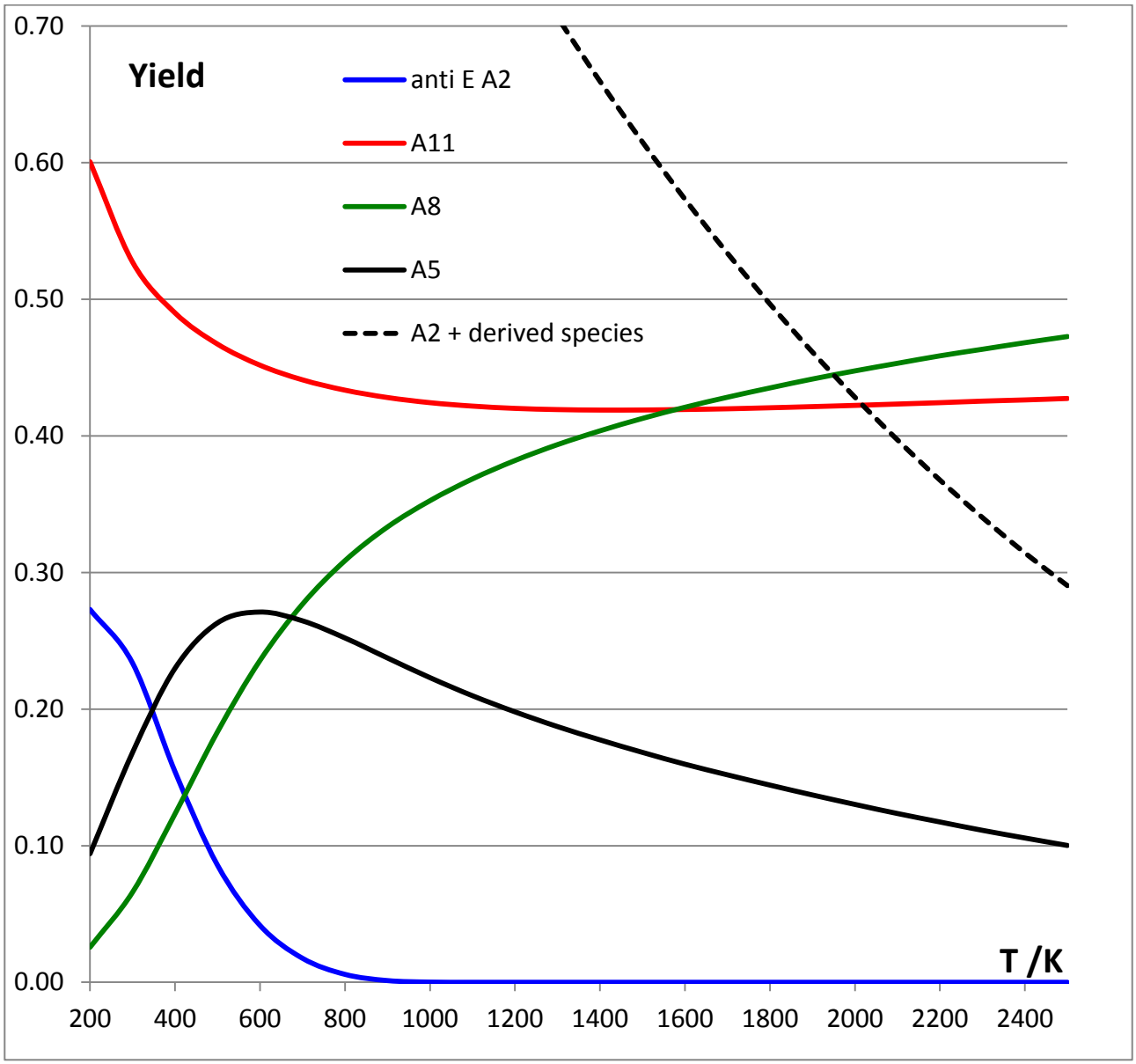

Figure 1. Reaction pathways started by hydroxyl addition to butadiyne. Continuous lines: net product reaction yields as a function of temperature. Labels make reference to Scheme 2. As higher T values are attained, the O_2 adducts tend to redissociate more effectively: the dashed black line (which stands alone) indicates the fraction of adduct that redissociates to **A2** + derivatives.

To consider a temperature range sufficiently wide to encompass combustion, post-combustion and emission in the atmosphere, the kinetic simulations were carried out as said in the range 200 K ≤ T ≤ 2500 K. The initial open-chain adduct anti E **A2** (a peroxyl radical intermediate) persists as important contribution (> 5 %) only below T ≈ 500 K, since it declines almost linearly right from the beginning as T rises (Figure 1). The contribution of the open chain tricarbonyl closed shell product **A11** mirrors the behavior of anti E **A2** in the rightmost part of the plot. Its yield attains a maximum in the 500-600 K zone. **A11** originates from anti E **A2** through unimolecular steps followed in the end by a hydrogen atom loss. Though fragmentation provides an entropic advantage to this step as T rises, other two fragmentation processes compete with it (compare Scheme 2). One entails the splitting of the molecular system into two almost comparable parts, formic acid, **A12**, and a radical

intermediate, **A13**. The second one implies hydroxyl loss and formation of a closed shell molecule, **A10**. The two pathways have very different weight at low T, with **A10** dominating over all other individual species. But their behavior is similar to that just described, and presents a crossing of the two curves around 1400 K, at which temperature their yield is ca. 40% each. Though intermediate ring products are present in Scheme 2, none of them plays an important role in Figure 1.

3.2 Reaction pathways started by hydroxyl H abstraction from butadiyne. RRKM-ME simulations show in this case that the only products are **B5** ($HC_3^{\bullet}$ + CO_2) and, to a lesser extent, **B10** ($HC_3^{\bullet}O$ + CO), at all temperatures considered. Higher temperatures further favor **B5**. These products are formed irreversibly, through fragmentations. In this case, in the range 1100-2500 K, the back-reaction to the reactants (**B1** + O_2) is negligible.

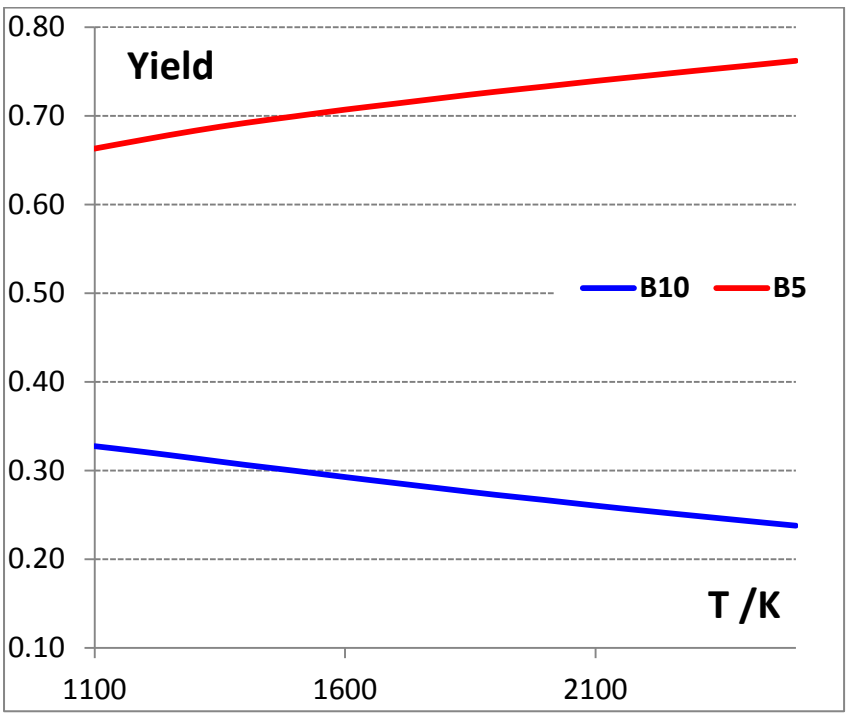

Figure 2. Reaction pathways started by hydroxyl H abstraction from butadiyne. Net product reaction yields as a function of temperature. Labels make reference to Scheme 3.

Conclusions

CCSD(T)/cc-pV*TZ* energetics have been defined for the HO + O_2 + C_4H_2 reacting system, based on the full study of the relevant DFT(M06-2X)/cc-pV*TZ* energy hypersurface. Then, two RRKM-ME simulations (A, B) have been carried out, in the temperature range 200-2500 K (P = 1 atm), to comprise the situations of emission into the troposphere and those typical of different combustions (Figure 1 and Figure 2).

Their results show that, when considering an initial HO addition to the triple bond of C_4H_2 (A) at rising T values, dioxygen takes part in C_4H_2 oxidation with decreasing efficiency, because at higher T values the O_2 adducts tend to redissociate. At T = 1800 K, for instance, the dioxygen adduct **A2** gives back the initial HO adduct **A1** and O_2 with a yield of ca. 50%. Let us begin by considering the gamut of rather low temperatures of environmental interest. These range approximately from 350 K down to ca. 200 K. These extremes correspond to going from a quite high ground-level temperature to that found close to the tropopause.[45] If T spans this range, two fragmentation species, HCOOH and $OC^{\bullet}$–C≡CH, **A8**, are predicted to be the main products of $HO^{\bullet}/O_2$ oxidation of butadiyne, together with two polycarbonyl molecules. These are: CHO.CO.C≡CH, **A5**, whose formation is accompanied by H loss; and CHO.CO.CH=C=O, **A11**, whose formation entails HO loss (see Figure 1 and Scheme 2). **A5**, **A8**, and **A11** are produced in irreversible steps. At the coldest temperatures, the initial adduct presence is significant, but its sharp declension upon temperature rise is also apparent. **A11** clearly dominates, but also declines as T rises. By contrast, both **A5** and **A8** gain importance by almost mirroring the trend of the other two species. They gain additional importance, as expected, as temperature further rises towards, and through, temperatures typical of combustion. **A8** yield constantly rises, whereas **A5** begins to decline beyond ca. 600 K, while **A11** decline comes gradually to a halt. Then, in the range 600 K < T < 1200 K), the density of the initial adduct **A2** drops to zero, and **A11** remains approximately constant. Thus, at combustion temperatures higher than 1200 K, **A8** and **A11** are described as the chief products of butadiyne oxidation, as far as hydroxyl addition followed by dioxygen addition define the initial steps.

However, at higher T, the starting point for dioxygen intervention can be instead the butadiynyl radical, $HC_4^{\bullet}$, formed by H abstraction operated by HO (B). New pathways, pertinent to combustion only, initiated by O_2 addition become then accessible and the RRKM-ME simulations indicate that the fragmentations to $HC_3^{\bullet}$ + CO_2 (**B5**) and $HC_3^{\bullet}O$ + CO (**B10**) are in this case the main outcome.

Acknowledgments. This work was conducted in the frame of EC FP6 NoE ACCENT and ACCENT–PLUS projects (Atmospheric Composition Change, the European NeTwork of Excellence).

Supporting Information for this article is available: it includes spin densities of some π–delocalized doublet intermediates, the geometries and energetics of all optimized structures, and the energetics at DFT(M06-2X)/cc-pv*TZ*.

References

1 Hansen, N.; Klippenstein, S. J.; Westmoreland, P. R.; Kasper, T.; Kohse-Höinghaus, K.; Wange, J.; Coole, T. A. *Phys. Chem. Chem. Phys.,* **2008**, *10*, 366–374.

2 Cordiner, M. A.; Charnley, S. B.; Buckle, J. V.; Walsh, C.; Millar, T. J. *Astrophys. J. Lett.* **2011,** *730:L18*, 1-5.

3 Homann, K.; Wagner, H.G. ,*Intl. Symp. Combust*., **1967**, **11**, 371.

4 Krestinin, A. V. *Combust. Flame* **2000**, 121, 513-524. Krestinin, A. V. *Chem. Phys. Rep.* **1998**, *17*, 1441-1461. Krestinin, A. V. *Chem. Phys. Rep.* **1994**, *13*, 191-210. See also: Indarto, A.; Giordana, A.; Ghigo, G.; Tonachini, G. *J. Phys. Org. Chem.* **2010**, *23*, 400-410.

5 Cahill, K. J.; Ajaz, A.; Johnson, R. P. *Aust. J. Chem.* **2010**, *63*, 1007–1012.

6 See for instance the following studies on their concentrations. **H, OH, CH_3:** Seepana, S.; Jayanti, S. *Energy Conv. Manag.* **2009**, *50*, 1116-1123. **H, O, HO, CH:** Choudhuri, A. R.; Gollahalli, S. R. *Int. J. Hydrogen Energy* **2004**, *29*, 1293-1302. **H:** Butler, C. J.; Hayhurst, A. N. *Comb. Flame* **1998**, *115*, 241–252. **H:** Bertagnolli, K. E.; Luchtb, R. P.; Bui-Pham, M. N. *J. Appl. Phys*. **1998**, *83*, 2315-2326. **HCO, HO, CH_2:** Lozovsky, V. A.; Derzy, I.; Cheskis, S. *Twenty-Seventh Symposium (International) on Combustion,* The Combustion Institute, **1998**, pp. 445–452. **O:** Barlow, R. S.; Fiechtner, G. J.; Chen J.-Y *Twenty-Sixth Symposium (International) on Combustion*, The Combustion Institute, **1996**, pp. 2199–2205. **HO:** Cheskis, S.; Derzy, I.; Lozovsky, V.A.; Kachanov, A.; Romanini, D. *Appl. Phys. B*, **1998**, 66*,* 377–381. **HO, NO:** Nguyen, Q. V.; Dibble, R. W.; Carter, C. D.; Fiechtner, G. J.; Barlow R. S. *Comb. Flame* **1996**, *105*, 499-510. **H, O, HO:** Zeegers , P. J. Th.; Alkemade, C. Th. J. *Radical recombinations & acetylene-air flames, vol. 9*, **1965**, 247-257.

7 Two pathways by which it can form are either from the ethynyl radical + ethyne reaction (Eiteneer, B.; Frenklach, M. *Int. J. Chem. Kinet*. **2003**, *35*, 391-414) or through H loss from the i-C_4H_3 radical intermediate ($H_2C{=}\dot{C}{-}C{\equiv}CH$). Of the following two reactions: $C_2H_2 + C_2H \leftrightarrows$ *n*-C_4H_3 (1), $C_2H_2 + C_2H \leftrightarrows$ *i*-C_4H_3 (2), the first one seems to be barrierless, hence more important [Ceursters, B.; Nguyen, H.M.T.; Peeters, J.; Nguyen, M.T. *Chemical Physics* **2000**, *262*, 243-252]. Then, H loss following (1) or (2) can give butadiyne (the reverse process was studied theoretically: Miller, S. J.; Klippenstein, J. A. *J. Phys. Chem. A* **2003**, *107*, 2680-2692). Otherwise, it can form directly via: $C_2H_2 + C_2H \leftrightarrows C_4H_2 + H$ (3).

8 Homann, K. H.; Warnatz, J.; Wellmann, C. *Symp. Int. Combust*. **1977**, *16*, 853-860.

9 Homann, K., H.; Schweinfurth, H. *Ber. Bunsenges. Phys. Chem.* **1981**, *85*, 569.

10 Warnatz, J. *Ber. Bunsenges. Phys. Chem.* **1983**, *87*, 1008-1022.

11 Krestinin, A. V.; Kislov, M. B.; Raevskii, A. V.; Kosoleva, O. I.; Stesik, L. N. *Kin. Catal.* **2000**, *41*, 90-98.

12 Hidaka, Y.; Henmi, Y.; Ohonishi, T.; Okuno, T.; Koike, T. *Comb. Flame* **2002**, *130*, 62-68.

13 Defoeux, F.; Dias, V.; Renard, C.; Van Tiggelen, P. J.; Vandooren, J. *Proc. Comb. Inst*. **2005**, *30*, 1407 -1415.

14 Li, Y.; Zhang, L.; Tian, Z.; Yuan, T.; Zhang, K.; Yang, B.; Qi, F. *Proc. Comb. Inst*. **2009**, *32*, 1293-1300.

15 Yang, B.; Li, Y.; Wei, L.; Huang, C.; Wang, J.; Tian, Z.; Yang, R.; Sheng, L.; Zhang, Y.; Qi, F. *Proc. Comb. Inst*. **2007**, *31*, 555-563.

16 Li, Y.; Zhang, L.; Tian, Z.; Yuan, T.; Wang, J.; Yang, B.; Qi, F. *Energy & Fuels* **2009**, *23*, 1473-1485.

17 Hansen, N.; Kasper, T.; Klippenstein, S. J.; Westmoreland, P. R.; Law, M. E.; Taatjes, C. A.; Kohse-Höinghaus, K.; Wang, J.; Cool, T. A. *J. Phys. Chem. A* **2007,** *111,* 4081-4092.

18 Li, Y.; Huang, C.; Wie, L.; Yang, B.; Wang, J.; Tian, Z.; Zhang, T.; Yang, R.; Sheng, L.; Qi, F. *Energy & Fuels* **2007**, 21, 1931-1941.

19 Musick, M.; Van Tiggelen, P. J.; Vandooren, J. *Comb. Flame* **1996**, *105*, 433-450.

20 Yokelson, R. J.; Burling, I. R.; Gilman, J. B.; Warneke, C.; Stockwell, C. E.; de Gouw, J.; Akagi, S. K.; Urbanski, S. P.; Veres, P.; Roberts, J. M.; Kuster, W. C.; Reardon, J.; Griffith, D. W. T.; Johnson, T. J.; Hosseini, S.; Miller, J. W.; Cocker, D. R. III; Jung, H.; Weise, D. R. *Atmos. Chem. Phys.* **2013**, *13*, 89–116.

21 For studies on planetary or satellite atmospheres, see for instance: Kunde, V.G. et alii *Science* **2004**, *305*, 1582-1586; (Saturn) de Graauw, T.; Feuchtgruber, H.; Bezard, B.; Drossart, P.; Encrenaz, T.; Beintema, D. A.; et alii *Astron Astrophys* **1997**, *321*:L13–6; (Uranus) Burgdorf, M.; Orton, G.; van Cleve, J.; Meadows, V.; Houck, J. *Icarus* **2006**, *184*:634–7. (Titan) Shemansky, D.E.; Stewart, A. I. F.; West, R. A.; Esposito, L. W.; Hallett, J. T.; Liu, X. *Science* **2005**, *308*, 978–982. For C_4H_2 in C-rich protoplanetary circumstellar envelopes: Chernicharo, J.; Heras, A. M.; Tielens, A. G. G. M.; Pardo, J. R.; Herpin, F.; Guélin, M.; Waters, L. B. F. M. *Astrophys. J.* **2001**, *546*, L123-L126. Due also to this astrochemical interest, the photo-physical and chemical characteristics of C_4H_2 have been the subject of several studies.

22 Goldsmith P. F., et alii *Astrophys. J.* **2011,** *737*:96 (17pp).

23 Sittler, E. C. Jr.; Ali, A.; Cooper, J. F.; Hartle, R. E.; Johnson, R. E.; Coates, A. J.; Young D. T. *Plan. Space. Sci.* **2009**, *57*, 1547–1557.

24 Perry, R. A. *Comb. Flame* **1984**, *58*, 221-227**.**

25 Atkinson, R.; Aschmann, S.M. *Comb. Flame* **1984**, 58, 217-220.

26 Bartels, M.; Heinemann-Fiedler, P.; Hoyermann, K. *Z. Phys. Chem. N.F.* **1989**, *161*, 189-207.

27 (a) Senosiain, J. P.; Klippenstein, S. J.; Miller, J. A. *Proc. Comb. Inst*. **2007**, *31*, 185–192**.** See also their related papers: (b) Klippenstein, S. J.; Miller, J. A *J. Phys. Chem. A* **2005,** *109,* 4285-4295 (on the H + HC≡C–C≡CH reacting system) and (c) Senosiain, J. P.; Klippenstein, S. J.; Miller, J. A. *J. Phys. Chem. A* **2005**, *109,* 6045-6055 (on HO + HC≡CH).

28 At the DFT(M06-2X)/cc-pV*TZ* computational level, the 'HO addition to C2' transition structure is 5.9 kcal mol^{-1} above the reactants, to be compared to 0.1 kcal mol^{-1} for the addition to C1; the relevant adducts are located at -28.7 and -43.0 kcal mol^{-1}, respectively.

29 Pople, J. A.; Gill, P. M. W.; Johnson, B. G. *Chem. Phys. Lett.* **1992**, *199*, 557-560. Schlegel, H. B.; in *Computational Theoretical Organic Chemistry*, ed. Csizsmadia, I. G.; Daudel, R. Reidel Publishing Co., Dordrecht, The Netherlands, **1981**, pp. 129-159. Schlegel, H. B. *J. Chem. Phys.* **1982**, *77*, 3676-3681. Schlegel, H. B.; Binkley, J. S.; Pople, J. A. *J. Chem. Phys.* **1984**, *80*, 1976-**1981**. Schlegel, H. B. *J. Comput. Chem.* **1982**, *3*, 214-218.

30 Parr, R. G.; Yang, W. *Density Functional Theory of Atoms and Molecules*, Oxford University Press: New York, 1989, ch. 3.

31 Zhao, Y.; Truhlar, D. G. *Theor. Chem. Acc.* **2008**, 120, 215-41. Zhao, Y.; Truhlar, D. G. *Theor. Chem. Acc.* **2008**, 120, 215. Zhao, Y.; Truhlar, D. G. *Acc. Chem. Res*. **2008**, *41*, 157.

32 Kendall, R. A.; Dunning, T. H., Jr.; Harrison, R. J. *J. Chem. Phys.* **1992**, *96*, 6796-806.

33 Coupled cluster: Coester, F.; Kümmel, H. *Nucl. Phys.* **1960**, 17, 477. Cízek, J. *J. Chem. Phys.* **1966**, *45*, 650-654. Paldus, J.; Cízek, J.; Shavitt, I. *Phys. Rew. A* **1972**, *5*, 50-67. Pople, J. A.; Krishnan, R.; Schlegel, H. B.; Binkley, J. S. *Int. J. Quantum. Chem.* **1978,** *14*, 545-560. Bartlett, R. J., Purvis, G. D. *Int. J. Quantum. Chem.* **1978**, *14*, 561-581. Cízek, J., Paldus, J. *Phys. Scripta* **1980**, *21*, 251-254. Bartlett, R. J. *Ann. Rev. Phys. Chem.* **1981**, 32, 359-401. Purvis, G. D.; Bartlett, R. J. *J. Chem. Phys.* **1982**, *76*, 1910-1918. Scuseria, G. E.; Janssen, C. L.; Schaefer, H. F. III *J. Chem. Phys.* **1988**, *9*, 7382-7387. Scuseria, G. E.; Schaefer, H. F. III *J. Chem. Phys.* **1989**, *90*, 3700-3703.

34 Gaussian 09, Revision A.02, Frisch, M. J.; Trucks, G. W.; Schlegel, H. B.; Scuseria, G. E.; Robb, M. A.; Cheeseman, J. R.; Scalmani, G.; Barone, V.; Mennucci, B.; Petersson, G. A.; Nakatsuji, H.; Caricato, M.; Li, X.; Hratchian, H. P.; Izmaylov, A. F.; Bloino, J.; Zheng, G.; Sonnenberg, J. L.; Hada, M.; Ehara, M.; Toyota, K.; Fukuda, R.; Hasegawa, J.; Ishida, M.; Nakajima, T.; Honda, Y.; Kitao, O.; Nakai, H.; Vreven, T.; Montgomery, Jr., J. A.; Peralta, J. E.; Ogliaro, F.; Bearpark, M.; Heyd, J. J.; Brothers, E.; Kudin, K. N.; Staroverov, V. N.; Kobayashi, R.; Normand, J.; Raghavachari, K.; Rendell, A.; Burant, J. C.; Iyengar, S. S.; Tomasi, J.; Cossi, M.; Rega, N.; Millam, N. J.; Klene, M.; Knox, J. E.; Cross, J. B.; Bakken, V.; Adamo, C.; Jaramillo, J.; Gomperts, R.; Stratmann, R. E.; Yazyev, O.; Austin, A. J.; Cammi, R.; Pomelli, C.; Ochterski, J. W.; Martin, R. L.; Morokuma, K.; Zakrzewski, V. G.; Voth, G. A.; Salvador, P.; Dannenberg, J. J.; Dapprich, S.; Daniels, A. D.; Farkas, Ö.; Foresman, J. B.; Ortiz, J. V.; Cioslowski, J.; Fox, D. J. Gaussian, Inc., Wallingford CT, **2009**.

35 Holbrook, K. A.; Pilling, M.J.; Robertson, S.H. *Unimolecular reactions*. John Wiley & Sons, Chichester, **1996**.

36 Gilbert R. G., Smith S. C. *Theory of unimolecular and recombination reactions*. Blackwell Scientific, Oxford, **1990**.

37 MultiWell-2014.1, Jun 2014, software designed and maintained by Barker, J. R., with contributors Ortiz, N. F.; Preses, J. M.; Lohr, L. L.; Maranzana, A.; Stimac, P. J.; Nguyen, T. L.; Dhilip Kumar T. J.; University of Michigan, Ann Arbor, MI; http://aoss.engin.umich.edu/multiwell/.

38 Barker, J.R. *Int. J. Chem. Kinetics* **2001**, *33*, 232-245.

39 Barker, J.R. *Int. J. Chem. Kinetics* **2009**, *41*, 748-76

40 Eckart C. *Phys. Rev.* **1930**, *35*, 1303

41 Barker, J. R.; Shovlin, C. N. *Chem. Phys. Lett.* **2004**, *383*, 203-207.

42 A second epoxide ring closure comes out to be concerted with a C–C bond cleavage. Though conceivable, it produces an intermediate that is discarded because of its high energy.

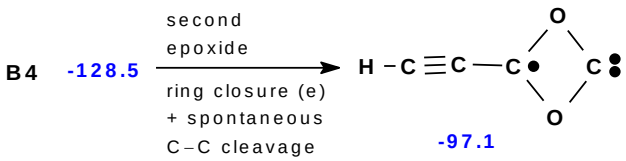

43 Up-down relationship: enantiomers (reflection with respect to the plane indicated by a horizontal dashed segment). Left-right: superimposable structures (through a π rotation around the x axis). Diagonal relationship: enantiomers (reflection with respect to sheet plane).

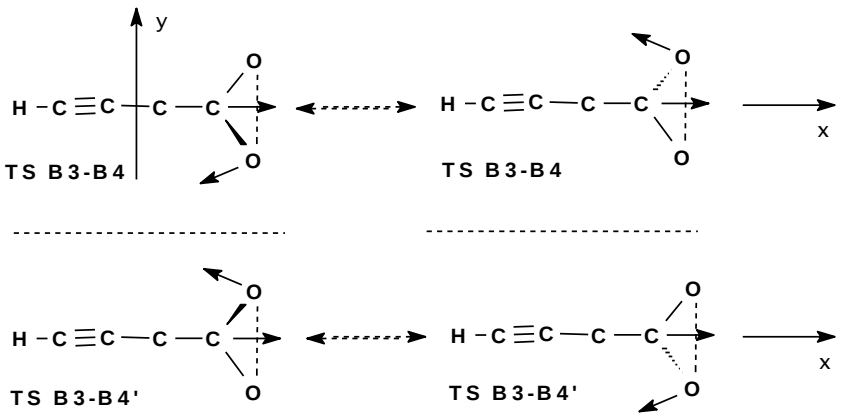

44 The *syn* and *anti* rotamers are separated by a barrier which is low enough to allow considering them collectively as a single well.

45 Hoinka, K. P. *Monthly Weather Rev.* **1999**, *127*, 2248-2265.